

# INFLUENCE OF GAS NITRIDING ON EROSION OF AISI 316L AUSTENITIC STAINLESS STEEL: PARAMETRIC STUDY

S. A. Hassona, F. M. Shuaeib, Ramdan O. Said<sup>\*</sup>, and K. F. Alabeedi

Mechanical Engineering Department, University of Benghazi, Libya

<sup>\*</sup>Mechanical and Industrial Engineering Department

University of Tripoli, Libya

E-mail: saied972004@yahoo.com

## المخلص

يعتبر البلى أو الحت السطحي بسبب الاحتكاك أو التصادم بجسيمات صلبة من الظواهر الشائعة في العديد من التطبيقات الصناعية وتتأثر هذه الظاهرة بالعديد من متغيرات التشغيل مثل زاوية الصدم وسرعة الحبيبات على عملية الحت. يقدم هذا البحث دراسة معمّلة لمعرفة تأثير عمليات تصليد الأسطح بواسطة النتردة، بغاز الأمونيا، على مقاومة الحت أو البلى الكشطي للصلب المقاوم للصدأ نوع (AISI 316L). تم استخدام الفحص المجهرى ودراسة حيود الاشعة السينية وجهاز لقياس صلادة الأسطح لفحص الطبقات المتكونة على سطح الصلب المقاوم للصدأ نتيجة النتردة. تمت عمليات النتردة بواسطة غاز الأمونيا في درجات حرارة بين 400 – 600 درجة مئوية وفي فترة زمنية من 10 الى 50 ساعة وفي معدل تدفق من 100 الى 600 لتر في الساعة. أظهرت نتائج الاختبارات أن عملية النتردة للصلب المقاوم للصدأ أنتجت طبقات متصلدة لسطح مقاوم للحت، حيث كانت متغيرة في السمك والبنية والصلادة وفقاً لشروط عمليات النتردة المختلفة. كما أظهرت الدراسة تحسن ملحوظ في مقاومة الحت للصلب المقاوم للصدأ المنترد مقارنة بالغير المنترد، هذا التحسن تأثر بزاوية الصدم التي هي ضمن متغيرات التشغيل المعتمدة في هذا البحث حيث اعتبر أن 93% من التحسن كان في اختبارات الزاوية 30 درجة وأن 59% من التحسن كان لزاوية 90 درجة.

## ABSTRACT

Erosion due to impact of hard and abrasive particles is a common phenomenon observed in many practical situations. A number of operating variables such as impact angle and impact velocity affect the erosion process. In the present work, AISI 316L austenitic stainless steel has been examined to study the effects of gas nitriding process parameters on its erosion wear resistance. Optical microscope, X-ray diffraction (XRD) and surface hardness measurements were used to investigate the properties of the nitrided layers produced during gas nitriding by ammonia in the range of (400–600°C) nitriding temperature, (10–50 hr.) nitriding time and (100-600 L/hr.) ammonia flow rate. The results of this study showed that gas nitriding of AISI 316L stainless steel produces nitrided layers that vary in thickness, composition and hardness according to the different nitriding conditions. Compared to the untreated material, the results of the erosion test show an improvement in erosion resistance after gas nitriding that can be related to the nitrided layer properties. This improvement in erosion resistance is dependent on the impact angle and could attain, within the range of process parameters considered in this study, a value of about 93% in the 30 ° test and 54% in the 90° test.

**KEYWORDS:** Erosion; Stainless Steel; Hardness; Nitriding Process

## INTRODUCTION

Among the different types of stainless steel, the austenitic types are the most widely used in chemical processing plants because of their high corrosion resistance in many environmental conditions and good mechanical properties. On the other side austenitic stainless steels have relatively low surface hardness and wear resistance. In practice, stainless steel components are subjected to surface damage by different forms of wear. For example, some well submersible pumps are manufactured in AISI 304 or AISI 316 stainless steels to meet the stringent requirements of the drinking water regulations. The extracted water is frequently loaded with abrasive substances, (e.g. sand), which are transported through all the fluid channels, the sidewalls of the impellers and all the close running clearances in the pump. Areas with high flow velocities, such as the narrow labyrinths, are exposed to the highest wear. If the size of the particles is less than the passage clearance, the particles move freely and impact the walls at a shallow angle. The result is erosion wear. On the other hand, if the particles are of the same size as the running clearances, they jam between the two walls and result in severe 3-body abrasion. Solid particle erosion caused due to the impact of high velocity particles entrained in a fluid stream is a common problem in a wide variety of machinery and industrial situations. Table (1) illustrates some other examples of components subjected to solid particle erosion either at room temperature or elevated temperature. This type of wear should be distinguished from the damage caused by other erosion forms like cavitation erosion, liquid impingement erosion and slurry erosion. The particles responsible for erosion are typically 5-500  $\mu\text{m}$  in size, and impact velocities can range from less than 10 m/s up to supersonic speeds.

**Table 1: Examples of components subjected to solid particle erosion [1]**

| System                     | Components                                                         |
|----------------------------|--------------------------------------------------------------------|
| Chemical plant             | Transport tubes carrying abrasive materials in an air stream       |
| Hydraulic mining machinery | Pumps and valves                                                   |
| Propellant system          | Rocket motors trail nozzle and gun barrel                          |
| Combustion system          | Burner nozzles, re-heater, super heater and economizer tubes banks |
| Fluidized bed combustion   | Boiler heat exchanger tubes, tube banks and expander turbine       |
| Coal gasification          | Turbine, lock hopper valves                                        |
| Coal liquification         | Valve for throttle the flow of product steam                       |
| Aircraft engine            | Compressor and turbine blades                                      |
| Helicopter engine          | Rotor and gas turbine blades                                       |

When a stream of solid particles is directed at a surface it is found that wear is dependent on the angle of incidence of the particles. This suggests two different mechanisms of erosion, dependent on whether the eroded solid is ductile or brittle. Figure (1) illustrates the variation of erosion rate with impact angle for two different materials. In the case of ductile materials, it is thought that the material removal mechanism near to the peak is through cutting and ploughing, while at angles close to 90° a fatigue mechanism is probably predominant. For brittle materials, subsurface cracks formed during particles impacts are linked together leading to material removal by flake fragmentation. In general, erosion rate is proportional to the kinetic energy of the impinging particles, that is, to the square of the velocity of the particles [2-4].

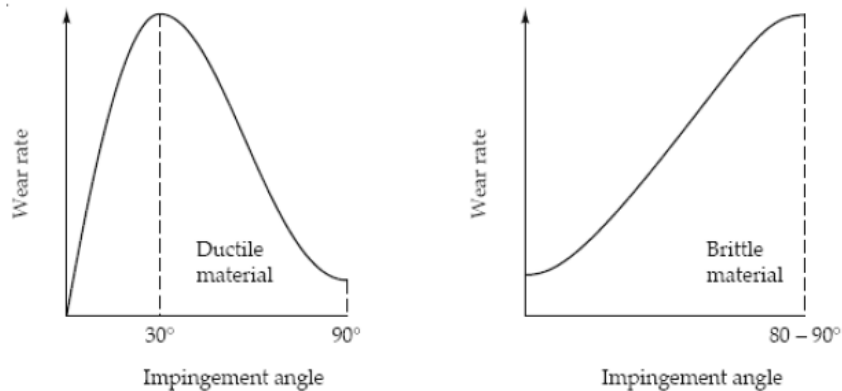


**Figure (1): Schematic representation of the effect of impact angle on wear rates of ductile and brittle materials [2]**

In order to improve the erosion wear resistance of austenitic stainless steels, they have to be surface hardened, which cannot be achieved by using carburizing or quenching heat treatments [5]. As an alternative, nitriding is an effective surface thermochemical treatment, which leads to a significant improvement in the surface hardness, wear resistance and fatigue strength [6]. Nitriding is widely used in automotive, mechanical and aeronautical engineering. Typical nitrided components are gears, crankshafts, camshafts, cam followers, and valves parts, die-casting tools, forging dies, aluminum-extrusion dies, extruder screws, injectors and plastic-mould tools. Literature survey on the nitriding of austenitic stainless steels shows that the nitriding process produces a high nitrogen-content surface layer with significant high hardness and improved wear properties [7-11]. It is found that the increase in surface hardness leads to higher erosion resistance as a result of the nitrided layer produced on the surface, especially at low impact angles [4]. The properties and composition of the nitrided layers are strongly influenced by a large number of processing parameters and recently, more research work is directed to study the nature of the S-phase, which forms at low nitriding temperatures [12-14].

In a previous study, it has been found that AISI 316L stainless steel is superior to AISI 304 and AISI 316 in its resistance to sensitization effect (IGC resistant) during gas nitriding at temperatures higher than about 450 °C. Therefore, the effect of gas nitriding by ammonia on the erosion wear resistance of AISI 316L austenitic stainless steel is studied in this work by utilizing response surface methodology (RSM) to determine the required experiments for effective modeling and analysis of results and to perform the nitriding process optimization. This statistical method is easy to apply and provides a comprehensive overview on the factors affecting a targeted response including interaction effects. The study also covers the effect of gas nitriding processing parameters on the microstructure, composition and surface hardness of the nitrided layers formed on the stainless steel surface.

## **MATERIALS AND METHODS**

AISI 316L stainless steel samples of chemical composition listed in Table (2) were cut from commercially available rod of 16 mm diameter in the form of discs with a thickness of about 5 mm. The samples, in the as-received condition, were solution annealed at 1050 °C for 60 minutes followed by oil quench. SiC abrasive papers down to 500-grit were used to manually ground the samples surface to achieve a fine finish.

**Table 2: Chemical compositions (wt %) of the materials used (Fe balance)**

| Alloy     | C    | Si   | S    | P    | Mn  | Ni   | Cr   | Mo  |
|-----------|------|------|------|------|-----|------|------|-----|
| AISI 316L | 0.03 | 0.46 | 0.02 | 0.02 | 1.8 | 11.2 | 16.0 | 2.0 |

The samples were gas nitrided in a pit type industrial furnace (SIB 572) by using 100% ammonia gas, anhydrous (UN 1005) with a minimum purity of 99.5 %. The nitriding process was conducted with varying three processing parameters which are temperature ( $^{\circ}\text{C}$ ), time (hr) and ammonia flow rate (L/hr). The number of experiments and the processing parameters setting for each experiment were determined using RSM to obtain a proper experimental design with minimum number of experimental points as given in Table (3). The preparation of nitrided specimens to metallographic examination was carried out with referring to the ASTM E3-80 standard [15]. ZEISS-Axiovert10 light-optical microscope was used to investigate the microstructure of the nitrided layers while the layers thickness measurements were taken by the micrometer provided with LEICA-VMHT microhardness tester used for the surface hardness measurements. The XRD patterns of nitrided specimens were obtained using PHILIPS-PW1800 x-ray diffractometer with  $\text{Cu K}\alpha$  radiation and 40 kV/10 mA generator setting. The erosion test was carried out on the air jet impingement tester shown schematically in Figure (2), which was built as per ASTM G76-83 standard [16].

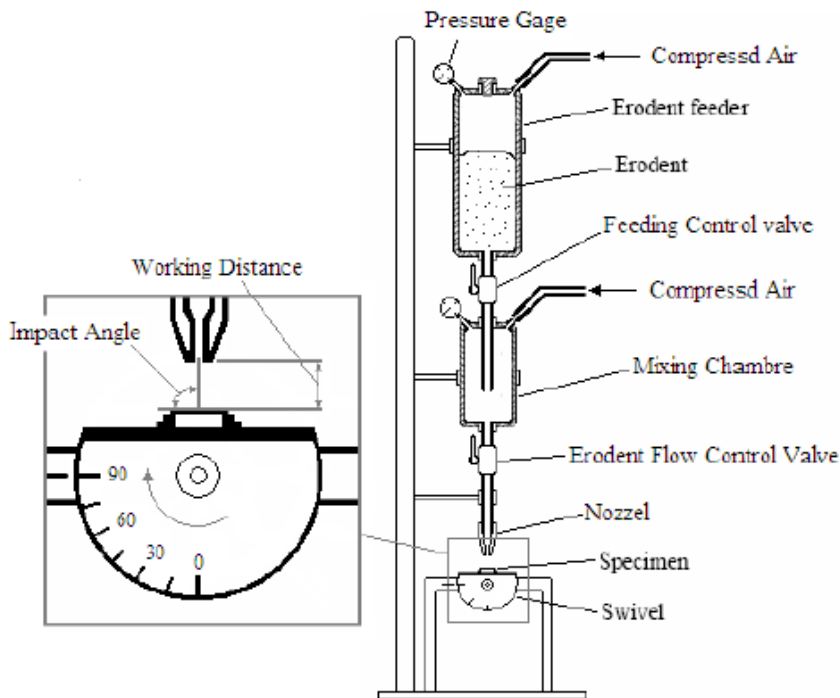


**Figure 2: Schematic for the erosion test apparatus**

Dry silica sand particles of different sizes in the range (400-600  $\mu\text{m}$ ) were used as eroder with an average impact velocity of about 50 m/s measured by double-disk method. The specimens were eroded in 3 min intervals for a total time of 18 min with a maintained working distance of 10 mm. The mass loss was measured to an accuracy of  $\pm 0.1$  mg using a precision digital balance.

## RESULTS AND DISCUSSION

### Microstructure observation and surface hardness results

The nitrided layers investigated by optical microscope vary in thickness and morphology depending on the nitriding process parameters. In the specimens treated at low temperatures (400 and 440 °C), uniform thin layers were observed which are not affected by the etching reagent and appear bright under microscope as shown by Figure (3-a). When increasing the nitriding temperature or time, the bright nitrided layers become dappled with dark spots (Figure (3-b)) and then, for higher temperatures (500 – 600 °C), the nitrided layers appear completely dark due to the heavy attack of the etching reagent as shown in Figure (3-c).

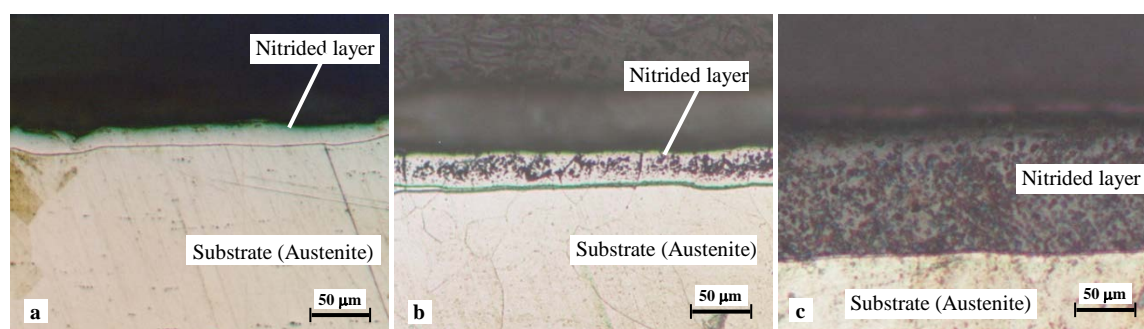


**Figure 3: Optical micrographs for nitrided layer morphologies; (a) design point #11, (b) design point #9, (c) design point #14**

Table (3) lists the layer thickness values, together with the corresponding layer morphologies. It can be seen from this table that as increasing the nitriding temperature in the range of 400 – 600 °C the resultant layer appearance changes from bright (DP #1, 5 and 11) to mixed (bright / dark) (DP #2, 6 and 9) and then to completely dark (DP #3, 4, 7, 8, 10 and 12-15). The same behavior is observed when nitriding time is increased from 10 to 50 hr., indicating that the bright layer formed at low nitriding temperatures decomposes at higher temperatures or by prolonged nitriding time. On the other hand, it seems that the flow rate of ammonia has negligible effect on the appearance of the nitrided layer.

The results of the surface hardness measurements on gas nitrided AISI 316L austenitic stainless steel in terms of  $HV_{0.1}$  are also obtained and presented as shown in Table (3). The results show that the surface hardness of the untreated material has been increased by about 520% which is of great importance in improving the wear resistance of the nitrided surfaces. It can be seen from this table, that increasing the setting of any processing parameter increases the surface hardness, but by different degrees. It is also noted that surface hardness values relatively decrease after certain levels of temperature and time are reached, which can be attributed to the coarsening of the fine nitrides particles presented in the nitrided layer.

### X-ray diffraction analysis

From the XRD analysis of nitrided AISI 316L stainless steels it was found that the phases present in the nitrided layers are related to the processing parameters, particularly the nitriding temperature. The XRD patterns of the specimens nitrided at 400 and 440 °C are dominated by a set of broad peaks, which appears at lower angles ( $2\theta$ )

than the substrate austenite peaks, as shown in Figures (4-a, b). These peaks, named S<sub>1</sub>, S<sub>2</sub> and S<sub>3</sub> could not be identified by the XRD index and are associated to the expanded austenite ( $\gamma_N$ ) or S-phase, as named by several investigators, which is reported to have excellent corrosion resistance [8-10, 14, 17].

**Table 3: Results of microscope investigation and surface hardness**

| design point | Time (hr) | Temperature (°C) | Flow rate (L/hr) | Layer thickness ( $\mu\text{m}$ ) | Layer morphology | Surface hardness (VH <sub>0.1</sub> ) |
|--------------|-----------|------------------|------------------|-----------------------------------|------------------|---------------------------------------|
| 1            | 18        | 440              | 200              | 15                                | Bright layer     | 755                                   |
| 2            | 42        | 440              | 200              | 23                                | Mixed layer      | 1026                                  |
| 3            | 18        | 560              | 200              | 122                               | Dark layer       | 1163                                  |
| 4            | 42        | 560              | 200              | 181                               | Dark layer       | 1139                                  |
| 5            | 18        | 440              | 500              | 18                                | Bright layer     | 972                                   |
| 6            | 42        | 440              | 500              | 40                                | Mixed layer      | 1144                                  |
| 7            | 18        | 560              | 500              | 133                               | Dark layer       | 1200                                  |
| 8            | 42        | 560              | 500              | 195                               | Dark layer       | 1243                                  |
| 9            | 10        | 500              | 350              | 37                                | Mixed layer      | 1159                                  |
| 10           | 50        | 500              | 350              | 159                               | Dark layer       | 1128                                  |
| 11           | 30        | 400              | 350              | 10                                | Bright layer     | 692                                   |
| 12           | 30        | 600              | 350              | 145                               | Dark layer       | 1129                                  |
| 13           | 30        | 500              | 100              | 90                                | Dark layer       | 1198                                  |
| 14           | 30        | 500              | 600              | 123                               | Dark layer       | 1202                                  |
| 15           | 30        | 500              | 350              | 78                                | Dark layer       | 1240                                  |
| 16           | 30        | 500              | 350              | 88                                | Dark layer       | 1191                                  |
| 17           | 30        | 500              | 350              | 82                                | Dark layer       | 1174                                  |
| Untreated    | -         | -                | -                | -                                 | -                | 200                                   |

In the XRD patterns of specimens containing mixed layers, CrN nitride is detected corresponding to the formation of the dark phase in the original bright nitrided layer as shown in Figure (4-c). In addition to the CrN peaks, the  $\gamma'$  – Fe<sub>4</sub>N nitride,  $\alpha$  (ferrite/martensite) and S-phase peaks are also found. When the nitriding temperature is increased above 500 °C, the dark nitrided layers produced have complex structures with various phases including  $\epsilon$ – Fe<sub>2-3</sub>N nitride,  $\gamma'$ , CrN, Cr<sub>2</sub>N,  $\alpha$  and interstitial N in  $\gamma$  as shown in Figure (4-d). From the XRD analysis it can be concluded that gas nitriding of AISI 316L austenitic stainless steel at low temperatures (less than 450 °C) produces bright nitrided layers which are precipitation free and consequently resist corrosion attack. These layers consist of a single phase named S-phase. When a critical temperature is reached CrN (dark phase) starts to precipitate in the original S-phase forming a mixed layer, and at higher nitriding temperatures, a dark layer is formed which is mainly composed of fine CrN precipitates in the austenite matrix.

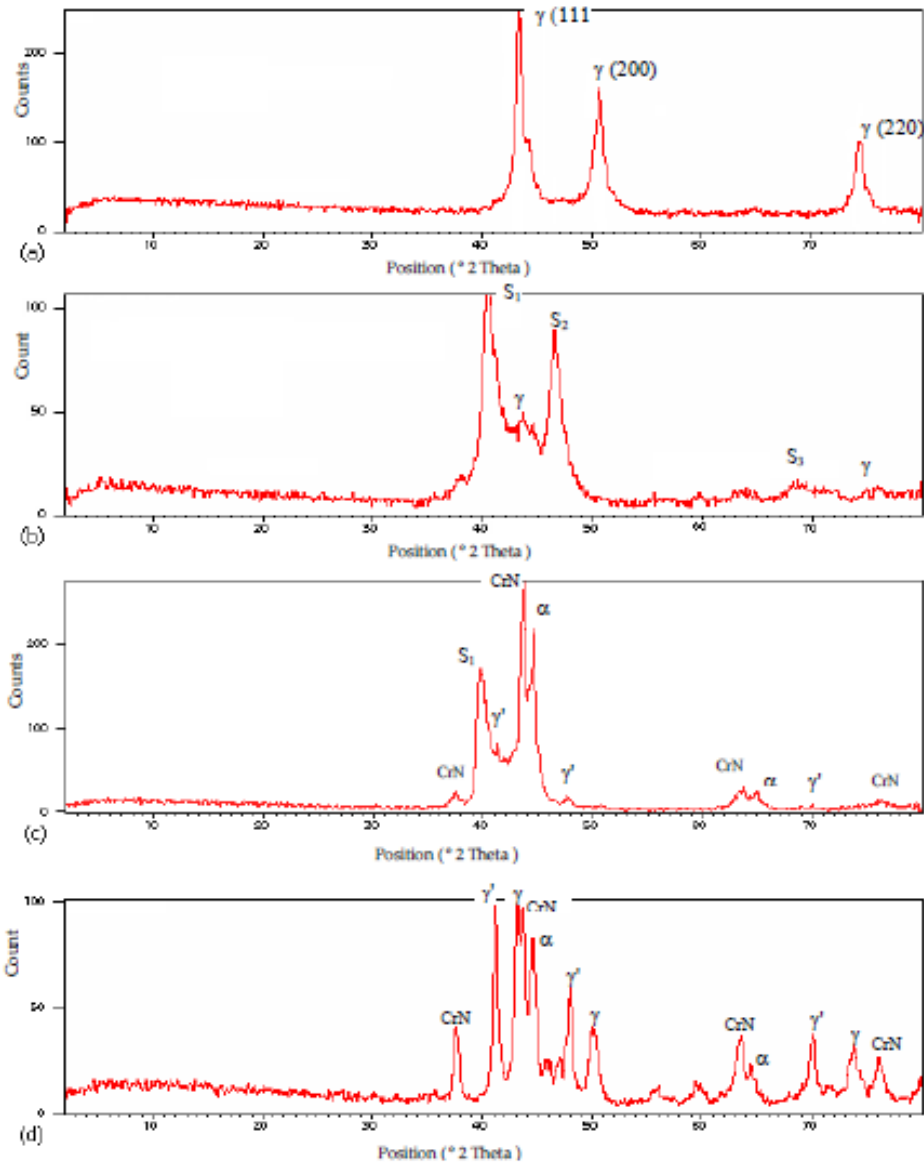


**Figure 4: XRD patterns of AISI 316L specimens: (a) untreated, (b) #11, (c) #9, (d) #8**

### Erosion Test Results

Erosion is often quoted in terms of mass removed from the surface by unit mass of erodent particles striking it (*milligrams eroded per kilogram of erodent*). This measure of erosion has the advantage that it is dimensionless, but for practical purposes, it is sometimes referable to express it as volume removed per unit mass of erodent (*mm<sup>3</sup> eroded per kilogram of erodent*) which is termed *erosion value* by the ASTM standard [16]. The results of erosion test performed on the gas nitrided AISI 316L austenitic stainless steel are inserted in the created RSM design matrix in terms of average erosion values (AEV) as shown in Table (4).

Compared with the untreated material, the results of AEV show an improvement in erosion resistance of about 87% for the 30° test and 46% for the 90° test. The standard design method *central composite design*, adopted in the well known MINITAB software, was employed for modeling and analyzing the influence of processing parameters on AEV.

**Table 4: AEV measurements of the nitrided AISI 316L**

| design point | Time (hr.) | Temperature (°C) | Flow rate (L/hr.) | AEV (30°) (mm <sup>3</sup> /kg) | AEV (90°) (mm <sup>3</sup> /kg) |
|--------------|------------|------------------|-------------------|---------------------------------|---------------------------------|
| 1            | 18         | 440              | 200               | 0.1167                          | 0.3056                          |
| 2            | 42         | 440              | 200               | 0.1203                          | 0.3425                          |
| 3            | 18         | 560              | 200               | 0.0742                          | 0.2314                          |
| 4            | 42         | 560              | 200               | 0.0842                          | 0.2500                          |
| 5            | 18         | 440              | 500               | 0.1044                          | 0.3333                          |
| 6            | 42         | 440              | 500               | 0.0742                          | 0.2408                          |
| 7            | 18         | 560              | 500               | 0.0808                          | 0.2442                          |
| 8            | 42         | 560              | 500               | 0.0725                          | 0.2408                          |
| 9            | 10         | 500              | 350               | 0.1111                          | 0.2964                          |
| 10           | 50         | 500              | 350               | 0.0556                          | 0.1758                          |
| 11           | 30         | 400              | 350               | 0.1389                          | 0.2964                          |
| 12           | 30         | 600              | 350               | 0.0742                          | 0.2131                          |
| 13           | 30         | 500              | 100               | 0.1019                          | 0.3333                          |
| 14           | 30         | 500              | 600               | 0.0978                          | 0.3056                          |
| 15           | 30         | 500              | 350               | 0.0842                          | 0.2869                          |
| 16           | 30         | 500              | 350               | 0.1019                          | 0.2686                          |
| 17           | 30         | 500              | 350               | 0.1028                          | 0.2608                          |
| Untreated    | -          | -                | -                 | 0.4353                          | 0.3242                          |

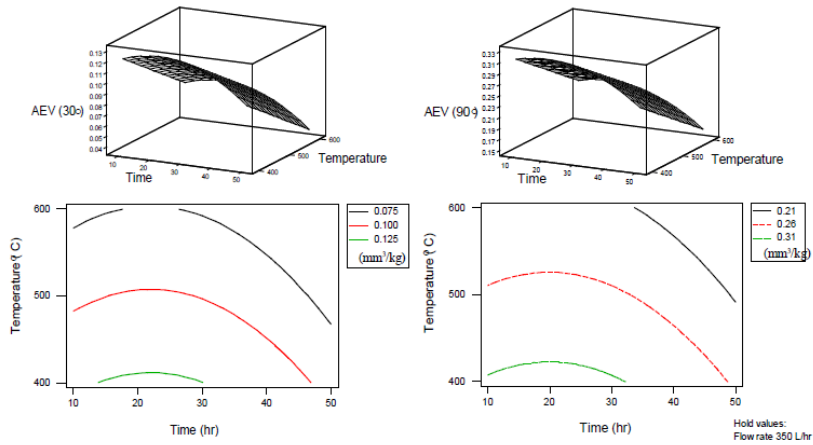
The statistical analysis of regression models shows that nitriding temperature and nitriding time have the most significant effects on the AEV response for the two tests, while the flow rate of ammonia dose not seems to have the same effect. After excluding the less significant terms, the statistical models for AEV can be presented by the equations:

$$AEV(30^\circ) = 0.313911 + 0.003252 t - 0.000519 T - 0.000296 q - 0.0000451 t^2 - 0.0000036 t \cdot q + 0.0000007 T \cdot q$$

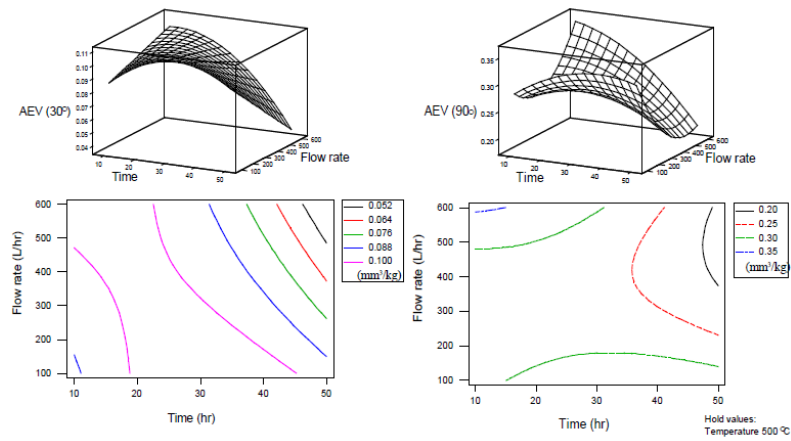
$$AEV(90^\circ) = 0.690158 + 0.006601 t - 0.000862 T - 0.000885 q - 0.0000734 t^2 + 0.0000008 q^2 - 0.0000105 t \cdot q + 0.0000011 T \cdot q$$

Where, **AEV (30°)** and **AEV (90°)** are the average erosion values at 30° and 90° impact angles respectively (mm<sup>3</sup>/kg), **t** is time (hr.), **T** is temperature (°C) and **q** is ammonia flow rate (L/hr.).

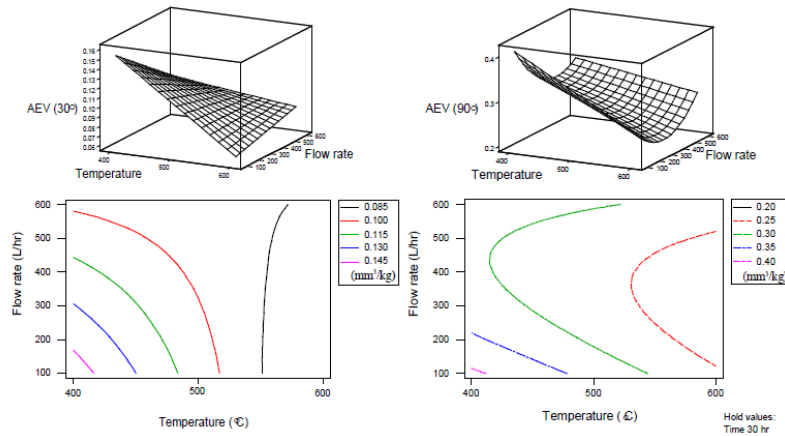
Based on the previous regression models, the effects of nitriding process parameters on the average erosion value are represented in the form of the 3D surfaces and contour plots shown in Figure (5). The results of the parametric study on the erosion rate of nitrided AISI 316L stainless steel could be discussed with the assistance of the nitrided layer microstructure, thickness and surface hardness results. The effect of temperature on reducing the AEV can be related to its role in increasing both of the surface hardness and nitrided layer thickness as can be seen from Table (3). The minimum AEV is attained in specimens nitrided at high temperatures and seems to be not affected by the relative decrease in surface hardness, which could be attributed to the high level (1000-1100 HV<sub>0.1</sub>) of surface hardness still maintained at high temperatures, in addition to the corresponding increase in layer thickness that improve the load-bearing capacity of the nitrided surface.



(a) The effect of time and temperature on AEV



(b) The effect of time and flow rate on AEV



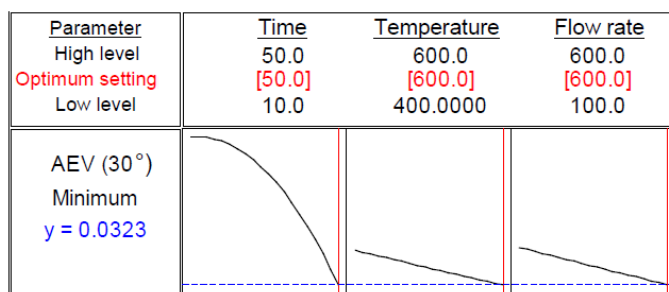
(c) The effect of temperature and flow rate on AEV

**Figure 5: The effect of nitriding process parameters on AEV**

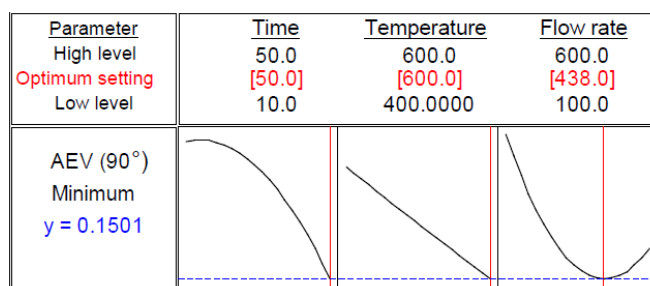
Regarding the effect of nitriding time in the range (10-22 hr.), the increase of AEV with increasing nitriding time is not consistent with the surface hardness results and may be attributed to the irregular nitrided layers formed when the nitriding period is short, or to the brittle compound zone which initially forms during nitriding. However, it is recommended that more investigation should be made to verify this

result. In the remaining part of the time range, AEV decreases as time increases and this is similar to the temperature effect. A significant difference between the results obtained from the two erosion tests appears when discussing the effect of ammonia flow rate. In the 30° test, increasing flow rate decreases the AEV due to contribution of flow rate in increasing the hardness and layer thickness. For nitriding temperatures higher than about 550 °C increasing flow rate increases the AEV probably due to the formation of a thick compound zone which is brittle and prone to be fractured by the striking erodent particles, and this can be supported by the XRD results which show high  $\gamma'$  and  $\epsilon$  peaks detected in the nitrided specimens with 500-600 L/hr. ammonia flow rate. In the 90° test the increase of AEV with increasing flow rate within the last half of the flow rate range could be discussed in the same manner since the relatively brittle compound zone is more affected by the higher impact angles. The effect of impact angle on the erosion performance explains the difference in AEV behavior of the nitrided layers between the two tests.

Using response surface methodology (RSM) provides the possibility to optimize the erosion test results of the gas nitrided AISI 316L stainless steel, which has been obtained by employing the response optimizer of MINITAB software. Figure (6) shows the optimization charts for the erosion test results. The predicted minimum AEV (30°) is found to be 0.0323 mm<sup>3</sup>/kg that can be attained by the parametric setting; 50 hr nitriding time, 600 °C nitriding temperature and 600 L/hr ammonia flow rate as can be seen from Figure (6-a). For the 90° erosion test, the predicted minimum of AEV (90°) is found to be 0.1501 mm<sup>3</sup>/kg with the parametric setting of 50 hr nitriding time, 600 °C nitriding temperature and 438 L/hr ammonia flow rate as shown by Figure (6-b). The parameters optimum settings are almost the same for both tests, and the predicted improvement in erosion resistance of nitrided AISI 316L can reach 93% in the 30 ° test and 54% in the in the 90° test.



(a) The response optimization for the minimum AEV (30 °)



(b) The response optimization for the minimum AEV (90 °)

**Figure 6: The optimization charts for AEV**

## CONCLUSIONS

Based on the results of this study it can be concluded that:

- The thickness, morphology and composition of nitrided layers formed in AISI 316L austenitic stainless steel depend on the nitriding process parameters.
- Gas nitriding for less than 30 hours at nitriding temperatures less than 450 °C produces nitrided layers, free of precipitates and mainly composed of S-phase which is reported to form during low-temperature plasma and ion nitriding.
- Gas nitriding of AISI 316L stainless steel significantly increases the surface hardness which has an important role in improving the resistance of material against solid particle erosion, particularly at low impact angles.
- The optimum improvement in the erosion resistance of type AISI 316L austenitic stainless steel by gas nitriding could attain about 93 % and 54 %, for the specimens tested at 30° and 90° impact angles respectively.
- RSM is a powerful method to study the gas nitriding effects on material surface properties, providing more information with fewer experiments and making a significant saving in time and cost.

## ACKNOWLEDGEMENT

The authors gratefully acknowledge the kind help in nitriding heat treatment and laboratory work offered by Eng. M. Al-Zorgani and Mr. A. Al-Mosbahi (The Technical Research Center – Mechanical Research branch, Tripoli) and by Mr. T. Al-Shelmani (University of Benghazi – ME dept. in Faculty of Engineering, Benghazi).

## REFERENCES

- [1] Sundararajan G. and Roy M., Solid Particle Erosion Behaviour of Metallic Material Room and Elevated Temperatures, *Tribology International*, 1997, vol. 30, no. 5, p. 335-359.
- [2] Stachowiak G.W. and Batchelor A.W., *Engineering Tribology*, 2006, (Butterworth-Heinemann Ltd, Oxford)
- [3] Hutchings I.M., *Tribology, Friction and Wear of Engineering Materials*, 1992, (Edward Arnold, London).
- [4] Divakara M., Agarwala V.K. and Singh S.N., Effect of the material surface hardness on the erosion of AISI 316, *Wear*, 2005, vol. 259, p. 110–117
- [5] Unterweiser P., Howard E. and James J., *Heat Treater's Guide, Standard Practices : Procedures for Steel*, 1982, (American Society for Metals, Metals Park, Ohio).
- [6] ASM Handbook Committee, *ASM Metals Handbook*, vol. 4, "Heat Treating", 1990 (ASM International Materials Park, Ohio).
- [7] Bell T., Surface Engineering of Austenitic Stainless Steel, *Surface Engineering*, 2000, vol. 18, no. 6, p. 415-422.
- [8] Poirier L., Corre Y. and Lebrun J., Solutions to Improve Surface Hardness of Stainless Steels Without Loss of Corrosion Resistance, *Surface Engineering*, 2002, vol. 18, no. 6, p. 439-442.

- [9] Ichii K., Fujimura K. and Takase T., Structure of Ion-Nitrided Layer of 18-8 Stainless Steel, Technology Report of Kansai University, 1986, vol. 27, p. 135-144.
- [10] Menthe E. and Rie K.T., Further Investigations of the Structure and Properties Austenitic Stainless Steel after Plasma Nitriding, Surface and Coatings Technology, 1999, vol. 116-119, p. 199-204.
- [11] De-Oliveira A., Riofano R., Casteletti L., Tremiliosi G. and Bento C., Effect of Temperature of Plasma Nitriding in AISI 316L Austenitic Stainless Steel, Rev. Brasileira de Aplicações de Vácuo, 2003, vol. 22, no. 2, p. 63-66.
- [12] Sun Y., Bell T., Kolosvary Z. and Flis J., The Response of Austenitic Stainless Steel to Low-temperature Plasma Nitriding, Heat Treatment of Metals, 1999, vol. 1, p. 16.
- [13] Yasumaru N., Nature of  $\gamma_N$  Phase Formed with Low Temperature Plasma Nitriding Austenitic Stainless Steel, Proceeding of Stainless Steel 2000 Conference, Osaka Japan, (Maney Pub.), 2001, p. 229-245.
- [14] Bell, T. and Li, C.X., Stainless Steel Low Temperature Nitriding and Carburizing, Advanced Materials and Processes, 2002, vol. 160, no. 6, p. 49-51.
- [15] ASTM Committee, "E3-80 Standard Methods of Preparing of Metallographic Specimens", Annual Book of ASTM Standards, 1988, vol. 03.01, p. 74-78. (ASTM Philadelphia).
- [16] ASTM Committee, "G76-83 Standard Practice for Conducting Erosion Tests by Solid Particle Impingement Using Gas Jets", Annual Book of ASTM Standards, 1988, vol. 03.02, p. 325-329. (ASTM, Philadelphia).
- [17] Zhang Z.L. and Bell T., Structure and Corrosion Resistance of Plasma Nitrided Stainless Steel, Surface Engineering, 1985, vol. 1, no. 2, p. 131-136.